Elastohydrodynamic Properties of Seed Oils

G. Biresaw*

Cereal Products and Food Science Research Unit, National Center for Agricultural Utilization Research, ARS, USDA, Peoria, Illinois 61604

ABSTRACT: The film-forming properties of canola (CAN), soybean (SBO), and jojoba (JO) seed oils under elastohydrodynamic (EHD) conditions were investigated to determine whether differences in their chemical and physical properties affect their EHD properties. Polyalphaolefin (PAO), whose EHD properties have been reported before, was used as the reference synthetic oil. The effect of measurement variables (speed, load, and temperature) on the film thickness of seed oils was consistent with that predicted by EHD theory. Pressure-viscosity coefficients (pvc) calculated from film thickness data at 40°C showed a steady-state value until about 50 nm film thickness, from which the following mean and SD values for CAN, SBO, and JO were obtained (GPa^{-1}): 10.0 ± 0.9, 7.6 ± 0.7, and 7.3 ± 0.5, respectively. However, further reduction of film thickness below about 50 nm resulted in an increase of pvc for CAN, but a decrease of pvc for SBO and JO.

Paper no. J11274 in *JAOCS 83*, 559–566 (June 2006).

KEY WORDS: Boundary lubrication, canola oil, elastohydrodynamic (EHD) lubrication, jojoba oil, lubricant film thickness, mixed-film lubrication, optical interferometry, polyalphaolefin, pressure-viscosity coefficient, soybean oil.

Biobased materials are manufactured using feedstocks originating from plants and/or animals (1). They differ from petroleum-based materials in that they have an unlimited and renewable raw material base. Also, they are generally nontoxic and environmentally friendly. As a result, biobased materials form the basis for the manufacture and use of a variety of "green" products. Examples of biobased raw materials include agricultural products such as starches, proteins, fats, and oils.

An important area of application for biobased products is in lubrication (2,3), particularly with plant-based oils or seed oils. Certain physical and chemical properties of seed oils make them attractive as lubricants. For example, their liquidity at room temperature allows them to be used as base oils for formulating lubricants used in various applications. Their amphiphilicity (4), i.e., having one or three polar ester groups distinctly separated from one or three long nonpolar hydrocarbon groups (5–7), allows them to be used as film-strength additives in lubricant formulations. Being both liquid and amphiphilic allows seed oils to be used as functional fluids, i.e., fluids that can provide both film thickness and film strength, in lubricant applications. In spite of these advantages, seed oils have several drawbacks to their use in lubricant formulations (8–11), including poor oxidative stability, poor bioresistance, and high pour points. Chemical modifications of the seed oils (e.g., hydrogenation) and/or the incorporation of various additives (e.g., antioxidants, pour point depressants, biocides) can overcome these drawbacks in seed oil-based lubricant formulations (8–11).

Another problem with the use of seed oils in lubrication is their chemical variability (6,7,12). Even though seed oils can be broadly categorized as mono- or tri-esters (MAG or TAG), their specific chemical properties can be dependent on the source of the seed oil. These differences arise from variations in the chemical structures of the FA and fatty alcohol residues of the mono- and tri-esters comprising the seed oils. As a result, seed oils vary in both their polar and nonpolar segments of the molecules. The polar segment can be mono- or triester. The nonpolar segment can have wide-ranging differences in hydrocarbon chain length (C_{12}–C_{26}), degree of unsaturation (0–3), position of unsaturation, and stereochemistry of unsaturation (*cis, trans*). In addition, some seed oils (e.g., castor oil, lesquerella) contain functional groups (e.g., hydroxy, epoxy) on the hydrocarbon chains. The chemistry, position, and number of functional groups on the hydrocarbon chain can also vary (12).

An important aspect of tribological research on seed oils is that of understanding the effects of chemical variability on lubrication properties. Most lubrication processes occur in the mixed film regime (13), in which both the boundary and hydrodynamic properties of the lubricants play critical roles. To understand the tribological properties of seed oils, one must know the effect of seed oil chemical variabilities on their boundary and hydrodynamic properties.

We have investigated the effect of chemical properties of seed oils on their boundary properties (4,14–16). The effect of variability in the polar and nonpolar segments of seed oils on their adsorption properties onto steel surfaces was investigated using (i) the friction method, developed by Jahanamir and Beltzer (17,18), and (ii) the interfacial method, developed in our group (16). The degree of adsorption of seed oils was quantified using the Gibbs free energy of adsorption, ΔG_{ads}. The result showed that ΔG_{ads} decreased, i.e., showed stronger adsorption, with increasing degree of functionality of the polar group, as well as with increasing M.W. of the hydrocarbon segment (4,14–16).

We report here our investigation of the effect of seed oil chemical structures on hydrodynamic and elastohydrodynamic (EHD) properties of these oils. We considered the film-form-

*Address correspondence at Cereal Products and Food Science Research Unit, NCAUR, ARS, USDA, 1815 N. University St., Peoria, IL 61604. E-mail: biresawg@ncaur.usda.gov

ing properties of seed oils, i.e., their ability to form lubricant films of various thickness to separate the rubbing surface during a tribological process. Several methods are available for studying hydrodynamic and EHD properties (19,20). This study is based on optical interferometry.

EXPERIMENTAL PROCEDURES

Materials. All the oils investigated in this work were used as supplied. These were: canola oil (CAN; Cedar Vale Natural Health, Cedar Vale, KS); soybean oil (SBO; Pioneer Hi-Bred Intl., Des Moines, IA); jojoba oil (JO; USDA, Peoria, IL); polyalphaolefin oil (PAO; Durasyn 166; BP Amoco, Chicago, IL). Selected physical and chemical properties of these oils, along with their abbreviations, are summarized in Table 1. Isopropyl alcohol (99+%) and hexanes (99+%) used for cleaning instruments and specimens were obtained from Aldrich Chemical Company (Milwaukee, WI) and used as supplied.

Viscosity measurements. Dynamic viscosities were measured on an ARES LS-2 Rheometer, series #714106, firmware version 5.1, and equipped with Orchestrator 7.03 software (TA Instruments–Waters LLC, New Castle, DE). Measurement was conducted using 50-mm-diameter cone-and-plate geometry, with a cone angle of 0.0408 radians. Viscosity was measured at 40 and 100°C as a function of shear rate, which was varied from 100 to 10 s^{-1}. The effect of aging on dynamic viscosity of the oils was investigated on an AR 2000 Rheometer, version 5.2 firmware, and TA Instruments Advantage software version 4.3 (TA Instruments–Waters LLC,). This instrument is equipped with a Peltier plate heating/cooling system (TA Instruments–Waters LLC), capable of temperature control in the range −30 to 200°C. In the aging experiment, 60-mm-diameter aluminum parallel plates were used to measure dynamic viscosity as a function of time, for a duration of at least 1 h, at 150°C and a shear rate of 100 s^{-1}.

Kinematic viscosities at 40 and 100°C were measured following ASTM D 445 procedure.

Film thickness measurement. Lubricant film thickness was measured by optical interferometry between a glass disc and steel ball on an EHL Ultra Thin Film Measurement System (PCS Instruments, London, England). A brief description of the basic principles of this method is given next, followed by detailed descriptions of the instrument and procedure.

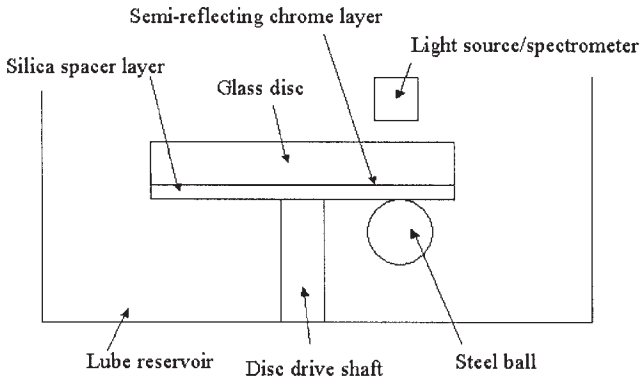

SCHEME 1

Basic principles of film thickness measurement using optical interferometry. Scheme 1 depicts the basic features of optical interferometry. The ball/disc contact is illuminated by a white light source directed down a microscope through the glass disc onto the contact. The bottom of the glass disc is coated with a semireflecting chrome layer that is coated with a silica spacer layer of known thickness. Part of the light is reflected from the chrome layer on the disc and part travels through the silica spacer layer and any fluid film and is reflected back from the steel ball. The two reflected light beams travel different distances and are combined, resulting in interference images, which are passed into a spectrometer and then into a high-resolution black and white CCD (charge couple device) camera. The camera image is captured by a video frame grabber and analyzed by the control software to determine film thickness.

The use of the spectrometer allows for the resolution of the interference image into a series of constructive and destructive fringes and for the precise determination of the respective wavelengths. The film thickness of the oil, h, is related to the wavelengths, λ, of the constructive fringes as described in Equation 1 (20):

$$h = [(N - \phi)\lambda]/[2\, n \cos(\theta)] \quad [1]$$

where $N = 1,2,3,\cdots$ is the fringe order, ϕ is net phase change due to reflection, n is the refractive index of the oil, and θ is the angle of incidence of the light beam (usually 0°).

TABLE 1
Some Physical and Chemical Properties of Oils Used in This Work

				Kin. viscosity, cSt		Unsaturation of FA residue, %					
Oil	Abbr.	Type	MW	40°C	100°C	18:1	18:2	18:3	20:1	22:1	24:1
Canola	CAN	TAG	879	39.5[a]	8.5[a]	60.9[b]	21[b]	8.8[b]	1.0[b]	0.7[b]	
Soybean	SBO	TAG	869	32.7[a]	7.5[a]	23.3[b]	53.7[b]	7.6[b]			
Jojoba	JO	MAG	606	22.6[a]	6.4[a]	9.0[c]			70[c]	14.0[c]	3[c]
PAO	PAO	Non-functional		31[d]	5.9[d]	None	None	None	None	None	None

[a]This work.
[b]Reference 7.
[c]Average values from Abbott, T. (USDA, Peoria, IL; 2001, unpublished data).
[d]Certificate of analysis (BP Amoco, Chicago, IL; 2004).

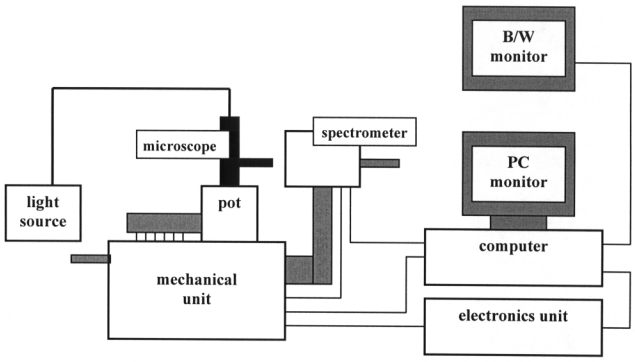

SCHEME 2

The use of a silica spacer layer of known thickness (~500 nm) allows for the generation of interference images, even in the absence of lubricant film between the disc and ball, thereby allowing for the measurement of the thickness of ultrathin lubricant films. For further details see Reference 20.

Description of the instrument. The main components of the EHL Ultra Thin Film Measurement System are presented in Scheme 2. The main components of the instrument are: (i) the mechanical unit for generating lubricant film between the ball and disc at the required test condition; (ii) a light source/microscope for illuminating the contact zone with white light and collecting the reflected interference image; (iii) a spectrometer for resolving the interference image into a series of constructive and destructive fringes; (iv) a CCD camera for imaging the fringes; (v) a PC with a frame grabber and appropriate software (Ultra; PCS Instruments) for capturing the image from the CCD camera, calculating, displaying, and saving the film thickness data in real time; and (vi) an electronic unit, interfacing between the PC and mechanical unit, to allow for setting up test parameters (speed, load, temperature) and conducting the experiment using the PC.

The mechanical unit, which houses the glass disc and steel ball used in film thickness measurement, has the following main features: lubricant pot with a lubricant reservoir that allows for supplying, heating, and draining lubricant; main shaft connected to a motor by gearbox and pulley for securing and spinning the disc; ball carriage for securing the steel ball and allowing it to freely rotate with the disc during film thickness measurement; loading system bellows and locks for loading the ball against the disc; ball track micrometer for adjusting the track radius for the test; and spectrometer micrometer for adjusting the part of the spectrum displayed on the monochrome (B/W) monitor. In addition, the mechanical unit has the following features to allow for traction experiments: ball drive shaft, assembly, and adapter for connecting the ball to the ball drive motor; and traction transducer assembly for measuring torque during traction experiments

The disc used in film thickness measurement is float glass that is 100 mm in diameter by 12 mm thick and coated with about a 20-nm semireflecting chrome layer that in turn is coated with ~500-nm thick silica spacer layer. The super-finished precision steel ball has a diameter of 3/4″ (1.9 cm) and is made of G10 carbon Cr steel (AISI 52100). Other pertinent specifications of the instrument are: measured film thickness, 1–1000 ± 1 nm; rolling speed, 0–5 m/s; slide-to-roll ratio (SRR), 0–200%; applied load, 0–50 N; maximum contact pressure, 1.1 GPa (steel/steel), 0.7 GPa (steel/glass); lubricant temperature range, ambient to 150°C.

The ULTRA software carries out various tasks, ultimately measuring, saving, and displaying the film thickness data. Many of its tasks require operator input. The software is responsible for instrument calibration (temperature, speed, load, spectrometer, spectral response); setting up a directory for saving experimental test parameters and acquired data; inputting/setting up test variables (temperature, load, speed); applying and maintaining test conditions (temperature, load, speed) for each film thickness measurement; analyzing spectral images and determining the wavelength of maximum constructive interference; accepting or rejecting film thickness data based on the SD of three consecutive measurements under each test condition; measuring the thickness of the spacer layer (zero film thickness); measuring lubricant film thickness at the required test condition (temperature, speed, load); saving and displaying acquired speed vs. film thickness data, both graphically and in spreadsheet format, in real time; and ending the experiment, i.e., removing the load, stopping the rotation of the disc, and shutting off the heat to the lubricant/pot.

Film thickness measurement procedure. Film thickness test parameters were varied as follows: speed, 0.02 to 3.0 m/s in 20% increments; load, 10 to 40 N in 10 N increments; temperature, 30, 40, 70, 100, and 120°C

Prior to measurement, the lubricant reservoir/pot, steel ball, glass disc, and ball carriage are cleaned with isopropyl alcohol and hexane and allowed to dry. (The instrument was regularly calibrated for speed, load, spectral response, and temperature, and the spectrophotometer was also calibrated.) The ball track micrometer is adjusted to the test disc radius and locked in place, then the ULTRA program is started, a new test file is begun, and the proper test parameters are entered. The ball carriage is placed on top of the loading system and the lubricant added to the reservoir. The ball is carefully placed on the carriage to avoid transferring any lubricant onto the upper part of the ball. The glass spacer layer disc is secured and the pot lid positioned with the hole over the ball/disc contact area. The microscope assembly is then positioned so that the light source shines directly on the contact point between the ball and disc. The temperature controller is set to the desired test temperature (usually pot temperature), the disc speed set to zero, and the required load applied. The microscope and spectrometer are adjusted as needed to obtain a sharp spectral image on the monochrome display. The spectrometer micrometer is then used to move the order 3 intensity peak to the left side of the screen and the micrometer reading entered in the setup box of the software. “Smooth” and “peak fit” options are selected, and 75 points are used for peak fitting. The averaging bands are set so that the central portion of the contact image is between the two scroll bars. The “immediate” image feature of the software is then used to check whether the intensity peak is on the left side

of the spectrum intensity window. When the peak and its position are deemed satisfactory, the trigger point is selected to take images at this point on the disc. The current disc position from the disc micrometer is then entered into the program to set the "zero film" value and to calculate the disc spacer layer thickness. The desired starting speed and the percent speed increase per step are entered in the speed sequence menu. The load is set back to zero and the speed set to the first speed in the test sequence. When speed is attained, the load is increased to the desired value and temperature is monitored until it stabilizes at the set value. The program is set to take three images at the trigger point on consecutive rotations of the disc and to add data points automatically to the data set if the values are within the set limit of SD. The "Trig" button is then selected to begin acquiring the first data point as soon as the initial speed, load, and temperature are reached. More data are acquired by selecting speed increase followed by "Trig," until the peak moves off the screen. The acquired data points are automatically displayed graphically as well as on a spreadsheet showing speed in m/s, and film thickness in µm. Increasing speed and film thickness causes the intensity peak to move to the right, and eventually off the screen. When this happens, the peak is moved back to the middle of the screen without changing the speed from the last data point. This causes changes in the spectrometer micrometer reading. The new spectrometer micrometer reading is entered into the program and another data point is taken at the same speed. The order 3 peak is then moved to the right, until completely off the screen and the order 4 peak positioned to the left side of the screen. The correct spectrometer micrometer reading and order numbers are entered into the program and triggered to obtain another data point at the same speed. More data are obtained with the new order peak and increasing speed, as just discussed. Eventually, this order peak also will go off the screen, and the process continues with the next series of order peaks, until the maximum set speed. After acquiring the last data at the maximum speed, the load is set to zero and the disc stopped. The process is then repeated at the next required load and/or temperature. A fresh disc track and a new ball are used to run the set of experiments on each lubricant at all test conditions (various combinations of speed, load, and temperature). At the end of such an experiment, the lubricant is drained immediately, all components are cleaned, and the electronics are turned off.

RESULTS AND DISCUSSION

Viscosity of oils. The viscosity of the oils studied here displayed Newtonian behavior at both 40 and 100°C. This is illustrated in Figure 1, which examines the effect of shear rate on the viscosity of CAN. The dynamic viscosities of the oils at 40 and 100°C are summarized in Table 2.

The effect of aging on the dynamic viscosities of the oils was investigated at 150°C and a shear rate of 100 s^{-1} during a period of over 1 h. The results for the various oils are presented in Figure 2. PAO displayed a slight increase in viscosity during the first 15 min, after which it remained constant. All the seed oils displayed an increase in viscosity with time for the entire test period. SBO showed a steeper increase in viscosity with time than CAN or JO. This result is consistent with the relative degrees of unsaturation of these seed oils (see Table 1) and their propensity to oxidize/polymerize.

Effect of test parameters on lubricant film thickness. Film thickness was measured as a function of entrainment speed (u) of the lubricant between the glass disc and steel ball under pure rolling conditions, i.e., at zero SRR, and at various loads and temperatures. SRR and u are defined as follows:

$$u = (u_1 + u_2)/2 \quad [2]$$

$$\text{SRR} = |u_1 - u_2|/u = (2|u_1 - u_2|)/(u_1 + u_2) \quad [3]$$

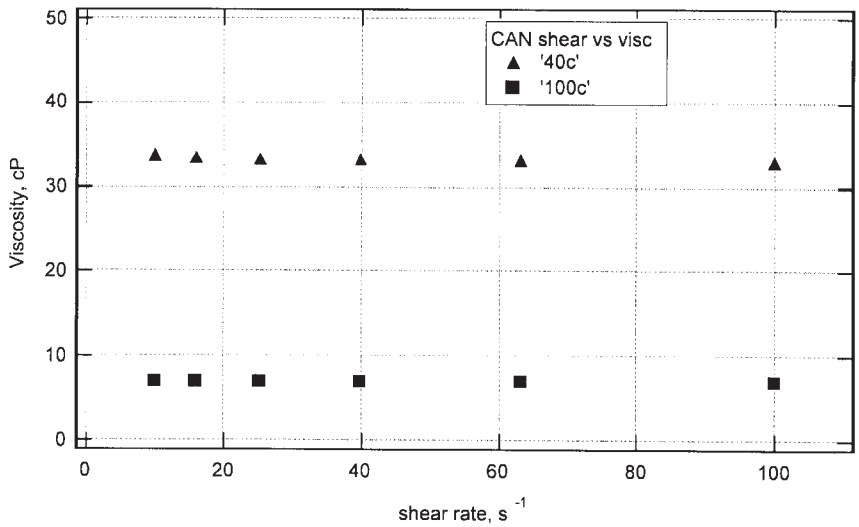

FIG. 1. Effect of shear rate on the viscosity of canola oil at 40 and 100°C.

TABLE 2
Dynamic Viscosities of Oils Used in Pressure-Viscosity Coefficient Calculations

Oil	Dyn. vis. at 40°C, cP	Dyn. vis. at 100°C, cP
PAO[a]	24.4[b]	4.5[c]
	24.4 ± 0.2[d]	4.4 ± 0.1[d]
CAN[e]	33.3 ± 0.2[d]	7.0 ± 0.1[d]
SBO[e]	30.3 ± 0.9[d]	7.3 ± 0.1[d]
JO[e]	21.2 ± 0.2[d]	5.30 ± 0.04[d]

[a]Reference fluid (see Eqs. 5 and 6 in text).
[b]Calculated from kinematic viscosity and density data (ASTM D 445), as reported in Reference 22.
[c]Extrapolated from calculated data at other temperatures in Reference 22.
[d]Measured, this work.
[e]Test fluid (see Eqs. 5 and 6 in text).

where u_1 and u_2 are the speeds of the disc and ball, respectively, in m/s.

Typical film thickness data for JO depicting the effect of speed and temperature are presented in Figure 3. These data were obtained at a load of 20 N, which corresponds to a contact pressure of 0.53 GPa between the steel ball and glass disc. The data indicate that film thickness h increases with increasing speed and decreasing temperature. Decreasing temperature increases the viscosity of the oil, which results in a thicker film. The result is consistent with EHD theory (21) on the effect of speed and viscosity on film thickness, as given in Equation 4:

$$h = k(u\eta)^{0.67}\alpha^{0.53} \quad [4]$$

where k is a constant that is dependent on test geometry and physical properties; η is dynamic viscosity at ambient atmospheric pressure in centipoise (cP), and α is the pressure-viscosity coefficient (GPa^{-1}) at the test temperature.

The data in Figure 3 show a linear relationship between log u and log h down to a speed of about 0.1 m/s (log $u = -1.0$), below which it deviates from linearity. This deviation is more pronounced at the higher temperatures and is attributed to changes in lubrication regime from EHD to mixed film (EHD/boundary) with decreasing film thickness (higher temperatures and slower speeds) (22). Linear regression of the film thickness data above 0.1 m/s gives a slope of about 0.7, which is consistent with the theory as given in Equation 4. As an example, the regression analysis of Figure 3 for the 40°C data of JO, gave a slope of 0.68 ± 0.01 ($R^2 = 0.99$). Similar results for the effect of speed and temperature on film thickness were obtained with the other oils used in this study.

Film thickness of soybean oil at 40°C is insensitive to changes in load, except below about 0.1 m/s, where some differentiation is observed (Fig. 4). This result is consistent with the expectation of the EHD theory as given in Equation 4, where the film thickness is independent of load. The slight load dependence observed at lower speeds could be due to a contribution from boundary lubrication (22).

Effect of lubricant properties on film thickness. Figure 5 compares the film thickness of the oils studied in this work at 40°C and 10 N load. The lubricants displayed similar film thickness trends in the entire speed range, which decreased in the order CAN > PAO > SBO > JO. The difference in film thickness between the lubricants, however, was not the same in the entire speed range. It was more or less constant until about a speed of 0.1 m/s, and showed significant divergence below this speed. The reason for this divergence could be due to change in the lubrication regime from EHD to mixed (EHD/boundary) (*c.f.* Figs 3 and 4).

The film thickness trends of seed oils studied in this work followed those of their viscosities at 40°C (Fig. 5; Table 1). The

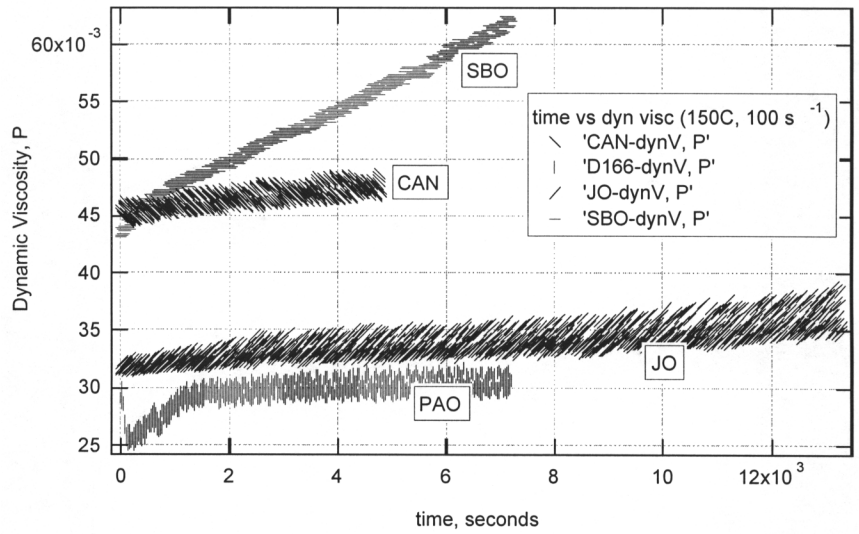

FIG. 2. Effect of heating time on the dynamic viscosity of lubricants used in this work (150°C, 100 s^{-1}). CAN, canola oil; D166, polyalphaolefin (BP Amoco, Chicago, IL); JO, jojoba oil; SBO, soybean oil.

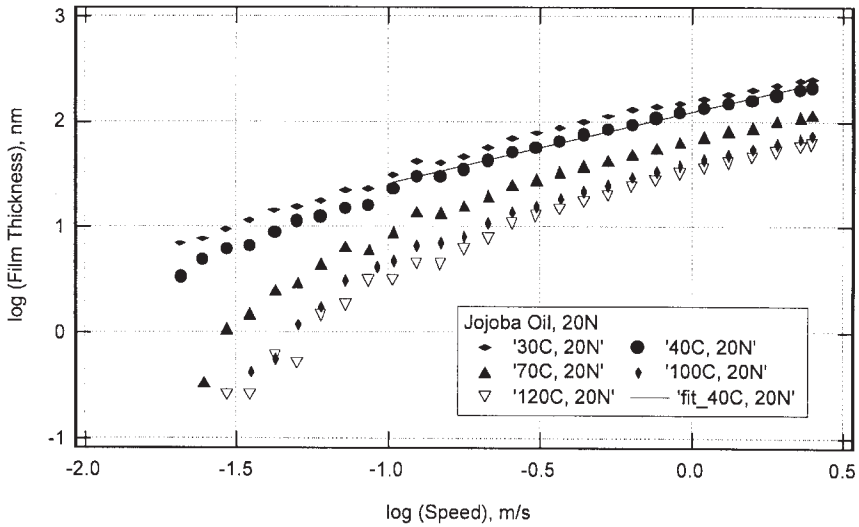

FIG. 3. Effect of temperature on the film thickness of jojoba oil.

measured film thickness increased with seed oil viscosity, which is consistent with expectations of the EHD theory (Eq. 4). However, the relative film thickness of PAO did not follow the relative viscosity shown in Table 1, as also predicted by the theory. Thus, even though PAO has a lower viscosity than SBO (Table 1), it produced a thicker film than SBO (Fig. 5), perhaps owing to differences in pressure viscosity coefficients of PAO vs. seed oils. These differences could in turn be due to differences in their chemical properties such as M.W., branching, degree of unsaturation, and number and type of functional groups.

The effect of lubricant viscosity on EHD properties has been extensively investigated and successfully modeled. However, few studies have considered the effect of lubricant structure on EHD properties. PAO is nonpolar whereas seed oils are polar. In addition, even though they are all polar, there are also differences in the structures among the seed oils used in this study, as summarized in Table 1. Whether structural differences affect the EHD properties of seed oils may be related to their pressure-viscosity coefficients,

Pressure-viscosity coefficient of seed oils. The pressure-viscosity coefficient of a test fluid (α_t) can be estimated from film thickness data of the test and reference fluids taken under identical test conditions (load, temperature, entrainment speed) (22). This estimate requires data on the pressure-viscosity coefficient of the reference fluid (α_r). The equation for this estimation is as follows:

$$\alpha_t = \alpha_r[(h_t/h_r)(a_r/a_t)]^{[1/0.53]} \quad [5]$$

where h_t and h_r are, respectively, film thickness of the test and

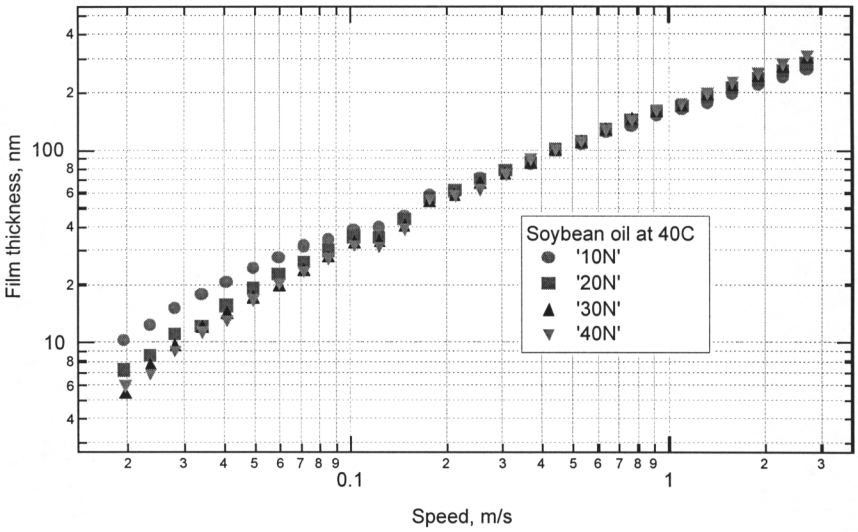

FIG. 4. Effect of load on the film thickness of soybean oil.

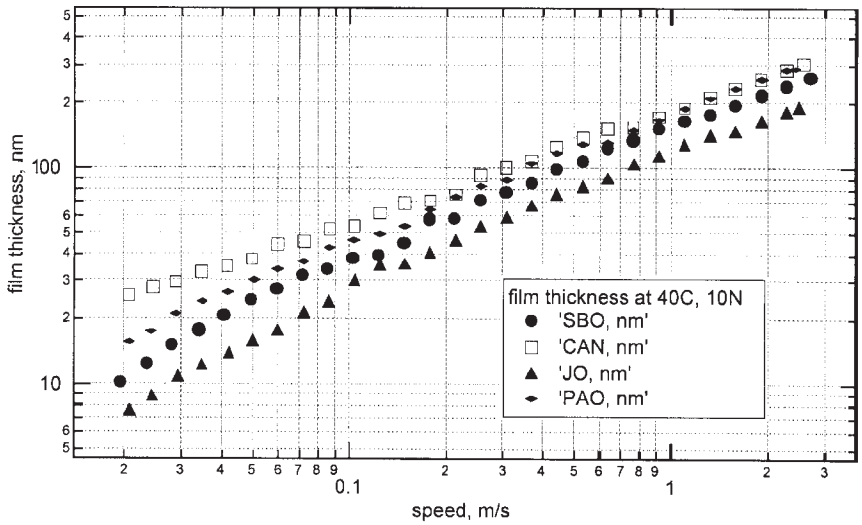

FIG. 5. Effect of lubricant chemical structure on film thickness at 40°C and 10 N. PAO, polyalphaolefin [= D166]. For abbreviations see Figure 2.

reference fluids under identical test conditions and a_t and a_r are the corresponding viscosity-speed parameters defined as follows:

$$a_t = (u_t\eta_t)^{0.67};\ a_r = (u_r\eta_r)^{0.67} \quad [6]$$

where u_t and u_r are, respectively, the entrainment speeds of the test and reference lubricants corresponding to h_t and h_r; and, η_t and η_r are, respectively, dynamic viscosities of test and reference fluids at ambient atmospheric pressure and test temperatures.

In this work, PAO was used as the reference fluid, since its pressure-viscosity coefficient as a function of temperature has been published (α_r = 13.5 GPa^{-1} at 40°C) (22). The dynamic viscosities of PAO and the seed oils used to estimate the pressure viscosities in Equations 5 and 6 are summarized in Table 2.

α_t values were calculated for each seed oil for the entire speed range of the film thickness data at 40°C and 10 N (Fig. 5). The results show that α_t remained nearly constant with decreasing film thickness until about 50 nm. Further reduction in film thickness resulted in an increase or decrease of α_t, depending on the seed oil. Values of α_t below a 50 nm film thickness increased with decreasing film thickness for CAN and decreased for SBO and JO.

Mean apparent pressure-viscosity coefficients of the seed oils, $<\alpha_t>$, were obtained by averaging the values in the steady-state region (h_t > 50 nm). The resulting values (GPa^{-1}) along with the SD at 40°C and 10 N were: 13.5 for PAO (22), 10.0 ± 0.9 for CAN (this work), 7.6 ± 0.7 for SBO (this work), and 7.3 ± 0.5 for JO (this work). The trend in $<\alpha_t>$ values at 40°C (CAN > SBO > JO) is similar to the trend in their film thicknesses (Fig. 5) and correlates with the corresponding viscosities (Table 2).

The observed relationship between film thickness below 50 nm and α_t of the seed oils, however, cannot be explained based on their differences in viscosity at 1 atm. One possible explanation for this observation could be the differences in the seed oil structures (Table 1). It is plausible that these differences could lead to differences in the way molecules from these seed oils organize in the confined space at the interface. These differences also could affect the response of these molecules to applied pressure under EHL conditions. Another possible explanation for the observed deviations between α_t and film thickness below 50 nm could be fractionation,

Fractionation in ultrathin films. Fractionation refers to the tendency of polar components of a lubricant to separate from the bulk and adsorb onto the rubbing surfaces as the film thickness decreases (23–27). The result is a deviation in the measured film thickness from that predicted for the bulk based on EHD theory. This deviation could be an increase or decrease in the film thickness, depending on whether the fractionating polar ingredient has a higher or lower viscosity, respectively, relative to the bulk. This has been clearly demonstrated by Guangteng and Spikes using polar ingredients with higher or lower viscosities than the bulk nonpolar base fluids (23). Fractionation is also related to the chemical functionality of the rubbing surfaces. Thus, little or no fractionation was observed on surfaces lacking adsorption sites (25). The effect of fractionation has also been observed on thin film properties derived from film thickness data (23,27). It has been demonstrated that inlet average effective viscosity and inlet relative average viscosity increased or decreased in line with the viscosity of the fractionating polar component.

As mentioned earlier, fractionation may explain the observed deviations between film thickness below 50 nm and pressure-viscosity coefficient of seed oils. If this is the case, all of the seed oils studied in this work displayed some degree of fractionation of a relatively more polar component than the bulk. The data also suggest that the fractionating component from CAN has a much higher viscosity than those from JO or

SBO. The possibility that these seed oils can undergo fractionation is not surprising, since it is well-known that commercial seed oils comprise mixtures of TAG and/or MAG of FA of various chemical structures (6,7). Commercial seed oils may also contain small quantities of long-chain FA and long-chain fatty alcohols owing to slow hydrolysis of these esters. Also, some of these components will be more polar than the bulk, and could have viscosities that are higher or lower than the bulk. Based on fractionation reasoning, the results suggest that polar components of CAN are more highly viscous than the bulk, whereas SBO and JO contain less viscous polar components.

At this time, it is not clear exactly what is responsible for the observed trend in the pressure-viscosity coefficients of the seed oils below about 50 nm film thickness.

ACKNOWLEDGMENTS

The author thanks Megan Goers, Andrew J. Thomas, and Armand Loffredo for their help with the experiments; Dr. Thomas Abbott for providing the JO sample; BP Amoco for providing the Durasyn 166 sample; and Drs. Ed Bagley and Dong Zhu for reviewing and commenting on this manuscript.

REFERENCES

1. Kaplan, D.L. (ed.), *Biopolymers from Renewable Resources*, Springer, Berlin, 1998.
2. Rhodes, B.N., and D. Johnson, Vegetable-Based Motor Oils, in *Biobased Industrial Fluids and Lubricants*, edited by S.Z. Erhan and J.M. Perez, AOCS Press, Champaign, IL, 2002, pp. 85–109.
3. Dwivedi, M.C., and S. Sapre, Total Vegetable-Oil Based Greases Prepared from Castor Oil, *J. Synth. Lubr. 19*:229–241 (2002).
4. Biresaw, G., A. Adharyu, S.Z. Erhan, and C.J. Carriere, Friction and Adsorption Properties of Normal and High Oleic Soybean Oils, *J. Am. Oil Chem. Soc. 79*:53–58 (2002).
5. Hiemenz, P.C., *Principles of Colloid and Surface Chemistry*, 2nd edn., Marcel Dekker, New York, 1986.
6. Bockish, M., *Fats and Oils Handbook*, AOCS Press, Champaign, IL, 1998.
7. O'Brien, R.D., *Fats and Oils: Formulating and Processing for Applications*, Technomics, Lancaster, PA, 1998, 694 pp..
8. Fox, N.J., A.K. Simpson, and G.W. Stachowiak, Sealed Capsule Differential Scanning Calorimetry—An Effective Method for Screening the Oxidation Stability of Vegetable Oil Formulations, *Lubr. Eng. 57*:14–20 (2001).
9. Miles, P., Synthetics Versus Vegetable Oils: Applications, Options, and Performance, *J. Synth. Lubr. 15*:43–52 (1998).
10. Becker, R., and A. Knorr, An Evaluation of Antioxidants for Vegetable Oils at Elevated Temperatures, *Lubr. Sci. 8*:95–117 (1996).
11. Adhvaryu, A., S.Z. Erhan, Z.S. Liu, and J.M. Perez, Oxidation Kinetics of Oils Derived from Unmodified and Genetically Modified Vegetables Using PDSC and NMR Spectroscopy, *Thermochim. Acta 364*:87–97 (2000).
12. Lawate, S.S., K. Lal, and C. Huang, Vegetable Oils—Structure and Performance, in *Tribology Data Handbook*, edited by E.R. Booser, CRC Press, Boca Raton, FL, 1997, pp. 103–116.
13. Schey, J. A., *Tribology in Metalworking: Friction, Lubrication and Wear,* American Society of Metals, Metals Park, OH, 1983, pp. 27–130.
14. Biresaw, G., A. Adhvaryu, and S.Z. Erhan, Friction Properties of Vegetable Oils, *J. Am. Oil Chem. Soc. 80*:697–704 (2003).
15. Kurth, T.L., G. Biresaw, and A. Adhvaryu, Cooperative Adsorption Behavior of Fatty Acid Methyl Esters from Hexadecane *via* Coefficient of Friction Measurements, *Ibid. 82*:293–299 (2005).
16. Biresaw, G., Adsorption of Amphiphiles at an Oil-Water vs. an Oil-Metal Interface, *Ibid. 82*:285–292 (2005).
17. Jahanmir, S., and M. Beltzer, An Adsorption Model for Friction in Boundary Lubrication, *ASLE Trans. 29*:423–30 (1986).
18. Jahanmir, S., and M. Beltzer, Effect of Additive Molecular Structure on Friction Coefficient and Adsorption, *J. Tribol. 108*:109–116 (1986).
19. Spikes, H.A., and P.M. Cann, Techniques for Studying the Behavior of Lubricants in Elastohydrodynamic Contacts, *Acta Tribologica 1*:33–48 (1992).
20. Johnston, G.J., R. Wayte, and H.A. Spikes, The Measurement and Study of Very Thin Lubricant Films in Concentrated Contacts, *Trib. Trans. 34*:187–194 (1991).
21. Hamrock, B.T., and D. Dowson, *Ball Bearing Lubrication: The Elastohydrodynamics of Elliptical Surfaces*, Wiley, New York, 1981.
22. Gunsel, S., S. Korcek, M. Smeeth, and H.A. Spikes, The Elastohydrodynamic Friction and Film Forming Properties of Lubricant Base Oils, *Trib. Trans. 42*:559–569 (1999).
23. Guangteng, G., and H. Spikes, Fractionation of Liquid Lubricants at Solid Surfaces, *Wear 200*:336–345 (1996).
24. Guangteng, G. ,and H.A. Spikes, The Control of Friction by Molecular Fractionation of Base Fluid Mixtures at Metal Surfaces, *Trib. Trans. 40*:461–469 (1997).
25. Spikes, H.A., Direct Observation of Boundary Layers, *Langmuir 12*:4567–4573 (1996).
26. Spikes, H., Advances in the Study of Thin Lubricant Films. New Directions in Tribology, *Plenary and Invited Papers from the World Tribology Congress,* 1st, London, Sept. 8–12, 1997, pp. 355–369.
27. Spikes, H.A., The Rheology of Very Thin Lubricant Films. Solid-Solid Interactions, *Proceedings of the Royal Society–Unilever Indo-UK Forum in Materials Science and Engineering,* 1st, London, 1996, pp. 334–351.

[Received November 9, 2005; accepted March 8, 2006]